CHAPTER-6

CONDUCTIVE-ATOMIC FORCE MICROSCOPY STUDY ON TiN_x AND $Ti_{1-x}Nb_xN$ THIN FILMS

Abstract

Simultaneous local current and topography measurements were made on the surface of TiN_x and $Ti_{1-x}Nb_xN$ thin films by conductive-atomic force microscopy (C-AFM). TiN_x (x=0.76, 1) and $Ti_{1-x}Nb_xN$ ($0 \leq x \leq 0.77$) thin films were deposited on borosilicate glass substrate using RF magnetron sputtering. Local variation of current at grain and grain boundaries was examined. Topography images reveal that the films consist of nano grains, for TiN_x films, the grain size is increased from 50 to 73nm as x increased from 0.76 to 1. Similarly, for $Ti_{1-x}Nb_xN$ films the value is increased from 30 to 90 nm as x increased from 0 to 0.77. In both type of films the current distribution on the surface also increased with increase in x for a constant applied voltage of 1V. The measured current is in the order of nA and its flow is filamentary in nature. Current-voltage characteristics of stoichiometric TiN reveal that the grain interiors are electrically conductive, while in sub-stoichiometric $TiN_{0.76}$ thin film, grains are electrically resistive, i.e., a potential barrier to electron transport exists at the junction between the grain and the grain boundary in sub-stoichiometric $TiN_{0.76}$. In $Ti_{1-x}Nb_xN$ films, the grains are electrical conductive and the I-V characteristics clearly show that the local resistance decreased with an increase in grain size. In both type of films, it is observed local resistance is several orders of magnitude larger than the total resistance and the value is of the order of MΩ. Electron-grain boundary scattering and the presence of native oxide states is responsible for increase the local electrical resistance of the films.

6.1 Introduction

Conductive Atomic Force Microscopy (C-AFM) is a mode of atomic force microscopy in which a conductive tip is scanned in contact with the conductive sample surface, while a dc voltage is applied between the tip and the sample, generating a current image. The electrical properties of granular materials such as thin films are strongly dependent on composition, crystallographic phase and microstructure. Microstructural features such as grain size, grain shape, grain boundary, porosity and roughness strongly affect the overall conductivity of the film. In addition, variations in local composition, electronic and electrical properties affect the overall performance and quality of nanostructures materials and devices. Conventional four-point probe method measures only the average value of electrical resistivity of a material at the macroscopic level. In contrast, conductive-atomic force microscopy (C-AFM) is a technique that can probe the local variations in the conductivity of a material (crystal or thin film) with microstructure. C-AFM has been widely used in profiling the local electronic structure and morphology of various surfaces with high spatial resolution. It is also possible to investigate quantitatively electron transport on a nm-scale by this technique [194-198].

In previous chapters IV and V, we have shown that microstructure, composition and physical properties of TiN_x and $Ti_{1-x}Nb_xN$ thin films are strongly dependent on process parameters. In this chapter, we present the C-AFM study of local electrical and electron transport properties of TiN_x and $Ti_{1-x}Nb_xN$ thin films of various compositions. A platinum thin film of thickness 40 nm was used as a standard for the topography and the C-AFM studies. The contribution of

grain interior and grain boundary to the total conductivity is clearly established by examining the current-voltage (I-V) characteristics across the scanned area.

6.2 Experimental condition

Table 6.1 Experimental conditions used to deposit TiN_x and $Ti_{1-x}Nb_xN$ thin films

Experimental parameter	**TiN_x**	**$Ti_{1-x}Nb_xN$**
Deposition method	RF magnetron sputtering	RF magnetron sputtering
Target material	2 inch diameter Ti	2 inch diameter Ti (Nb fractions was varied on the Ti surface)
Substrates	Borosilicate glass	Borosilicate glass
Ultimate pressure	3×10^{-6} mbar	3×10^{-6} mbar
Working pressure	5×10^{-2} mbar	5×10^{-2} mbar
Sputtering gas	100 % nitrogen	100 % nitrogen
RF power	100 Watt	100 Watt
IE Distance	60 mm	50 mm
Substrate temperature	200 and 350°C	250°C
Deposition time	120 min	120 min

The thickness of the films was estimated using surface profilometer and the values are 140 ±12 and 120±10 nm for TiN_x films deposited at 350 and 200°C and for $Ti_{1-x}Nb_xN$ films the value is 150±20nm. The composition of the films was determined from EDX spectra. For TiN_x films, deposited at 200 and 350°C, the composition determined as $TiN_{0.76}$ and TiN and for $Ti_{1-x}Nb_xN$ films the composition (x) values are 0, 0.26, 0.58 and 0.77 respectively. The structural properties of TiN_x and $Ti_{1-x}Nb_xN$ films are already been discussed in chapters 4 and 5.

6.3 Four probe measurement

The composition dependent sheet resistance of TiN_x and $Ti_{1-x}Nb_xN$ thin films was measured using the four probe technique at room temperature. The sheet resistance values for TiN and $TiN_{0.76}$ films are 12 kΩ/sq and 425 kΩ/sq respectively. In the case of $Ti_{1-x}Nb_xN$ thin films, the sheet resistance was calculated as a function of *x* and its variation depicted in figure 6.1. It is observed that the sheet resistance is decreased with increase in *x* value. The sheet resistance of TiN film for *x*=0 is 87 Ω/sq and this value is decreased to 72 Ω/sq for x=0.26, 27 Ω/sq at *x*=0.58 and finally 14 Ω/sq for *x*=0.77 in $Ti_{1-x}Nb_xN$ film. The detailed study of the composition dependent electrical resistivity of $Ti_{1-x}Nb_xN$ on SS substrate is already discussed in chapter-5. By comparing the sheet resistance values of TiN_x and $Ti_{1-x}Nb_xN$ thin films it is inferred that $Ti_{1-x}Nb_xN$ films are highly conductive than TiN_x films.

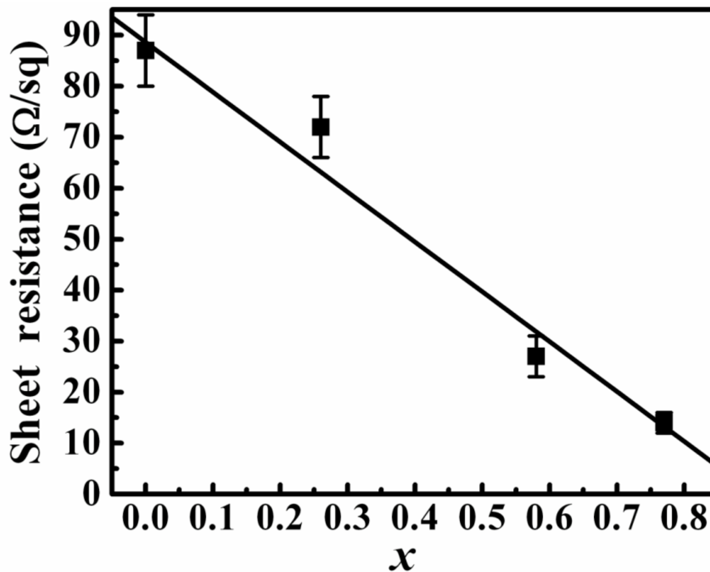

Figure 6.1 Variation of sheet resistance of $Ti_{1-x}Nb_xN$ thin films as a function of *x*

6.4 C-AFM measurement on the surface of TiN_x and $Ti_{1-x}Nb_xN$ thin films

6.4.1 TiN_x thin films

The 2-D and 3-D topography and current images of Pt, TiN and $TiN_{0.76}$ films are shown in figures 6.2 and 6.3. In both figures the left panel is topography image and the right panel is current image. From 2-D topography image, it is observed that the surface of the Pt film is relatively smoother (the average roughness being 0.84 nm) and less granular than that for the titanium nitride films.

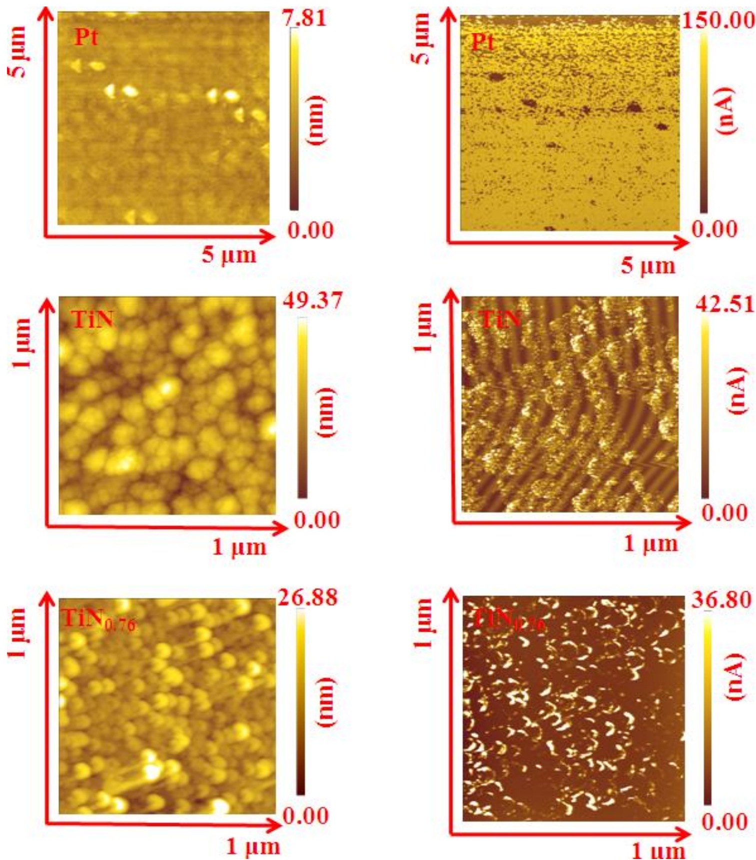

Figure 6.2: 2-D topography (left panel) and current (right panel) images of Pt, TiN and $TiN_{0.76}$ thin films

The titanium nitride films, on the other hand, were granular with some evidence for surface roughness. The grain size in the case of TiN was 73±12 nm with average roughness of 4±1 nm, while the grain size was 50±5 nm for the $TiN_{0.76}$ films with average roughness of 2±0.5 nm. In the 2-D current images bright areas correspond to regions of higher current flow.

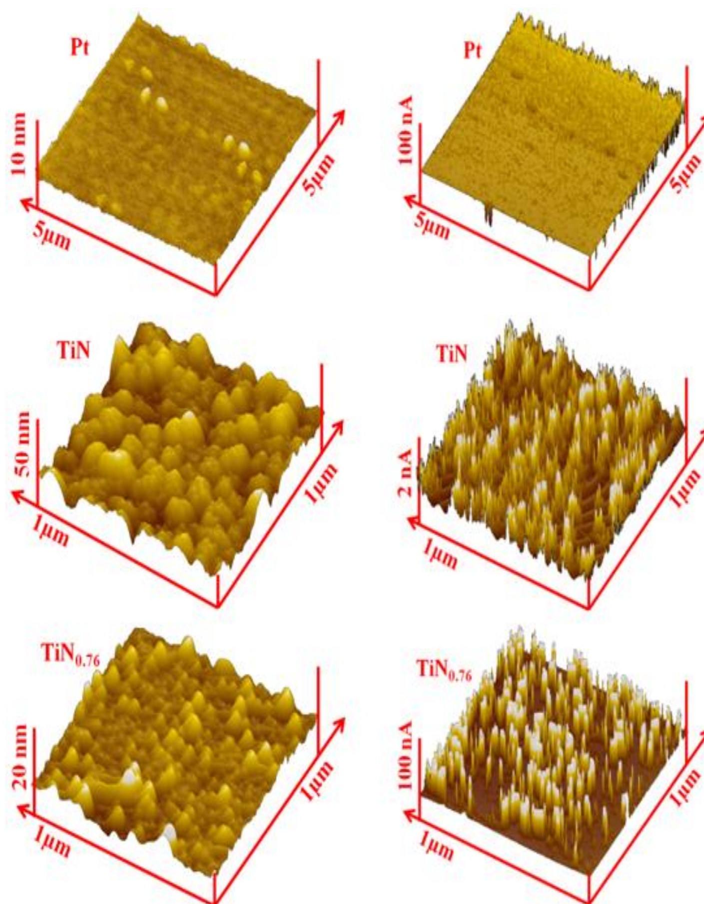

Figure 6.3: 3-D topography (left panel) and current (right panel) images of Pt, TiN and $TiN_{0.76}$ thin films

The current image was registered simultaneously with topography image at a constant voltage of 1 V applied to the sample during scanning. From 3-D current image (figure 6.3 right panel), it is observed that the current distribution across the surface of the Pt films is more uniform than that for the TiN_x films, with the maximum current (Z-axis) of ~75 nA. The mildly filamentary nature of the current distribution (especially at the edges) in this case can be attributed to the slight granularity and roughness of the surface. From the 3-D current images of the TiN and $TiN_{0.76}$ films, it is evident that the current flow across the two films is filamentary in nature, *i.e.* there are regions of high current are separated by regions of very low current. This is in sharp contrast with the current image of the Pt film which showed a uniform distribution of current across the film surface. But there is also a significant difference between the 3-D current images of the $TiN_{0.76}$ film, and that of the TiN film. Although in both the cases the current is filamentary in nature, the density of these filaments is much lower in sub-stoichiometric TiN films. Clearly, there are fewer percolation paths for conduction in $TiN_{0.76}$ than in stoichiometric TiN.

6.4.2 $Ti_{1-x}Nb_xN$ thin films

The C-AFM measurements were carried out on the surface of $Ti_{1-x}Nb_xN$ thin films similar to TiN_x films. The 2D topography images over a 1 μm ×1 μm scan area with the corresponding grain size distribution are shown in figure 6.4. From the figure, it is evidence that the surface of all films consists of spherical grains of slightly varying diameter without voids and rugged structure. The mean grain size (D) calculated from the grain size distributions shown in the same figure

indicate that the mean grain size increased with increase in x value. The mean grain size of TiN film for x=0 is 30 nm and the value is increased to 90 nm for x=0.77 in the $Ti_{1-x}Nb_xN$ thin film. Surface roughness also follows the same trend as grains size, the value is increased from 0.5 to 3.2 nm as x increase from 0 to 0.77. The grain size and roughness of thin films follow the linear relation; therefore, the grain size is responsible for the increase of roughness of the films [199]. The frequency of grain size is summarized in the form of histograms and all the films show an almost symmetric distribution. Histogram of all film is fitted to Gaussian (normal) distribution and the central tendency of the distribution is around mean grain size of the film.

Figure 6.5 shows the 2D and 3D current image of $Ti_{1-x}Nb_xN$ thin films over a 1 µm ×1 µm scan area. In the 2D and 3D current images, bright the areas correspond to areas of higher conductivity than the darker low conductivity areas. Hence, by comparing the 2D topography and current images, the conducting/insulating paths on the surface of the films can be distinguished. There is significant variation in the 3D current images of $Ti_{1-x}Nb_xN$ film with increasing value of x. From the 3D current images it is observed that the current on the surface increased with increase in grain size. TiN film having grain size of 30 nm shows a maximum current on the surface is 15 nA (Z-axis). The current value increased to 37 nA and then to 85 nA for $Ti_{1-x}Nb_xN$ films with x=0.26 and 0.58 having grain sizes of 42 nm and 75 nm respectively. The maximum current of 100 nA was observed for the $Ti_{1-x}Nb_xN$ with x=0.77 and grain size 90 nm. It should be noted that the maximum current may be higher but shows saturation since the current pre-amplifier in our C-AFM system saturates at 100nA. Similar to TiN_x films, current flow in

$Ti_{1-x}Nb_xN$ films also have filamentary nature. From figure 6.5, it is observed that the grain interiors are conductive than the grain boundary.

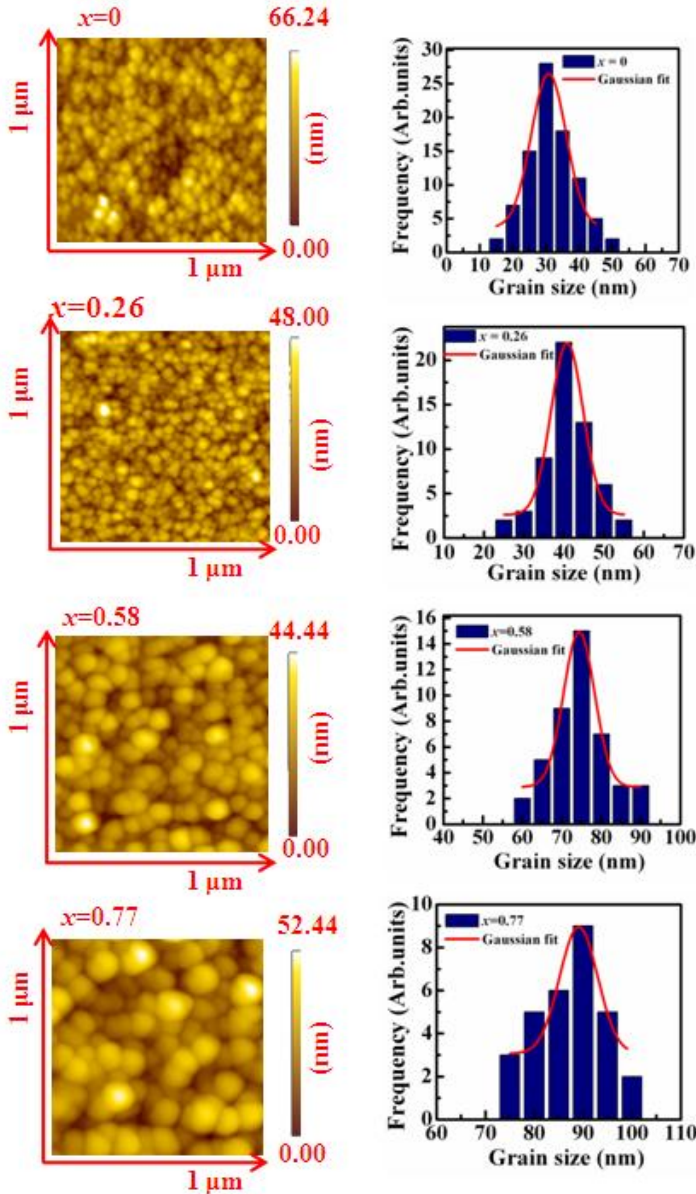

Figure 6.4: 2-D topography images of $Ti_{1-x}Nb_xN$ thin films over 1 µm ×1 µm scan area with corresponding grain size distribution.

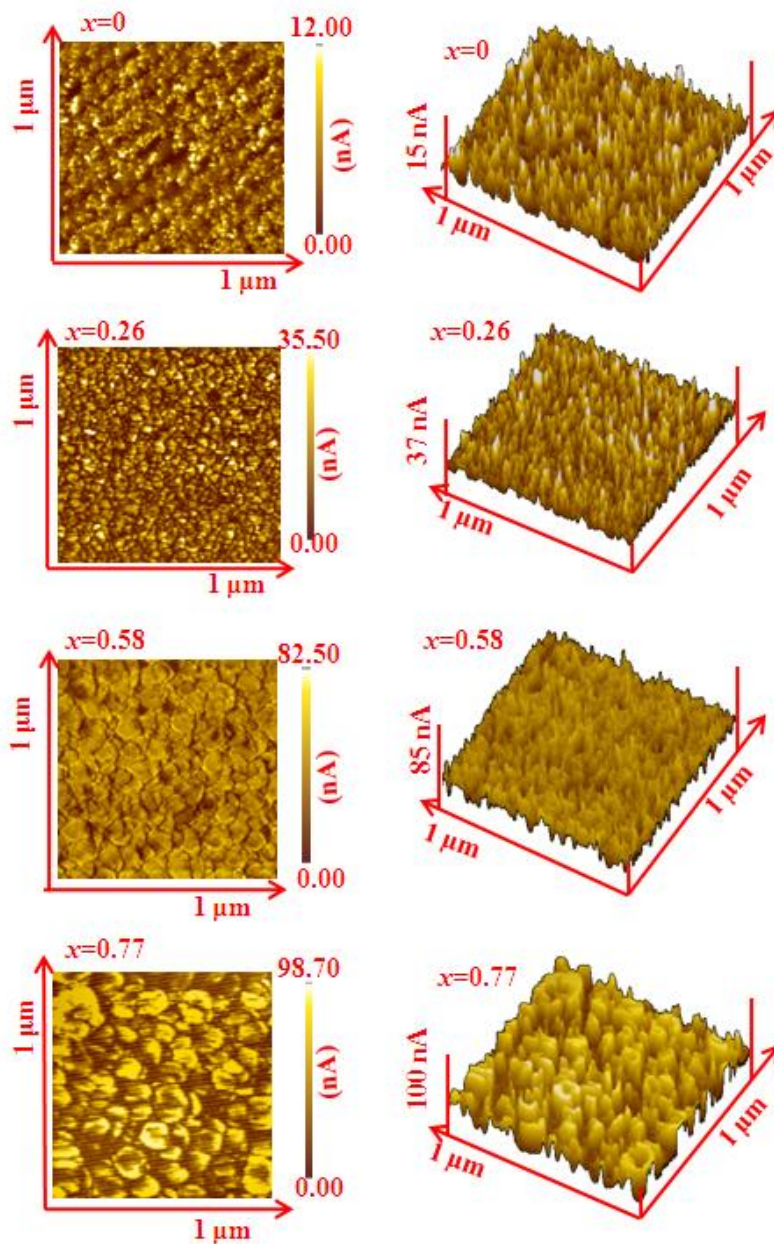

Figure 6.5: 2-D (left panel) and 3-D (right panel) current image of $Ti_{1-x}Nb_xN$ thin films

6.5 Local electrical and electron transport properties of TiN_x and $Ti_{1-x}Nb_xN$ films

6.5.1 Local I-V characteristics of TiN_x and $Ti_{1-x}Nb_xN$ films

Local I-V characteristics of TiN_x and $Ti_{1-x}Nb_xN$ films are measured at different locations across the scanned area of each film *in-situ* after imaging. The I-V characteristics of TiN_x films along with platinum film are shown in figure 6.6. The 2-D current images with locations at which the I-V characteristics were measured are also given in these figures as insets. The I-V characteristics of the Pt film indicate that the film is uniformly conducting across the scanned area. This view is supported by the ohmic nature of the I-V plots at all locations considered. In the case of the stoichiometric TiN films, the I-V characteristics reveal that the grain interior and grain boundary conductivity is of the same order of magnitude, but non-ohmic. At a bias of 0.05 V, the current is of the order of 50 nA, leading to a local resistance of the order of 1 MΩ. In addition, the conductivity saturates at higher bias voltages (>0.1 V). For the sub-stoichiometric $TiN_{0.76}$ films the situation is completely different. The current in the grain interiors at a given bias (locations 1, 2, 3 and 4) is much lower than the current in the grain boundaries (locations 5 and 6). There is almost one order of magnitude difference in conductivity. Within the grains (locations 5 and 6) the resistance of the order of 1 MΩ, whereas across the grain boundary the conductivity is diode-like with an energy barrier (i.e., the minimum bias at which conductivity commences) of the order of 0.6 V.

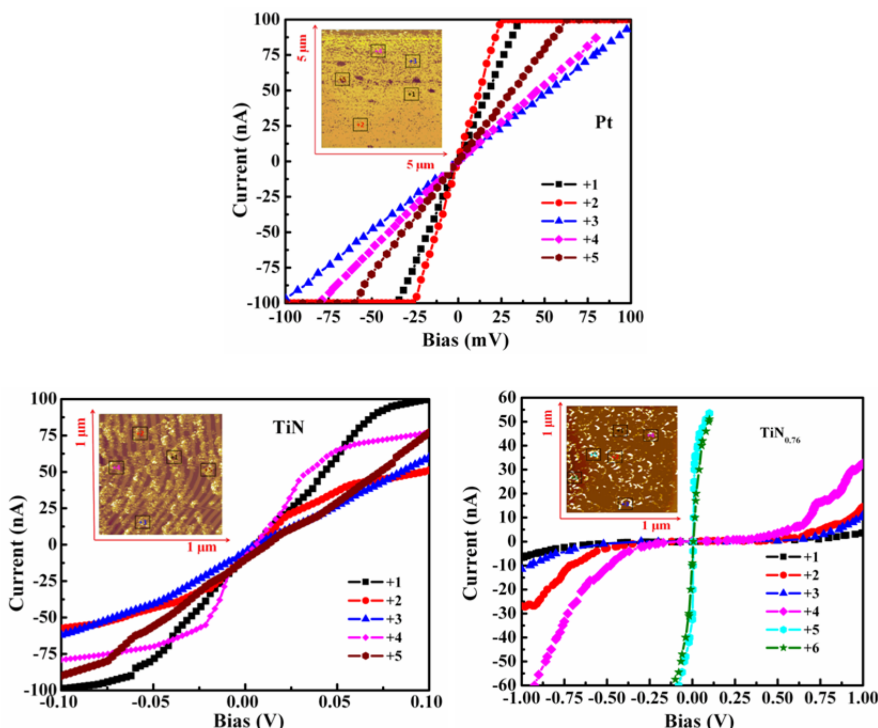

Figure 6.6 I-V characteristics of the Pt, TiN, and $TiN_{0.76}$ films taken at different locations on the current image shown in the insets

Figure 6.7 shows the local I-V characteristics of $Ti_{1-x}Nb_xN$ films for a sweeping voltage of ± 100 mV. For TiN film (x=0), the I-V characteristics were measured at high and low conducting areas. Points selected at high conducting area (+1 and +2), I-V curve shows Ohmic behavior while the low conducting area (+3) shows non-linear behavior. The resistance (1/slope) of the curves slightly varied and the magnitude of current on the y-axis was in the range of 5-20 nA at a bias voltage of 100 mV. Since the tip diameter is 35 nm, in this case it may be in contact

with both grain and grain boundary, as the mean grains size (30nm) of the films is less than that of radius of curvature of the tip. Hence, it is not possible to distinguish the grain and grain boundary contribution to the resistance. Therefore, the resistance measured from I-V curves of TiN film is due to both grain and grain boundary contribution. In the case of $Ti_{1-x}Nb_xN$ film (x=0.26), the I-V characteristics of all points selected (+1, +2 and+3) display Ohmic behavior. The magnitude of current on y-axis is around 30 nA at a bias voltage of 100 mV. The grain size of the film is 42 nm, therefore, in this case the tip is partially in contact with grain and grain boundary. Similar variation in I-V characteristics of $Ti_{1-x}Nb_xN$ film for x=0.58 is observed. However, the magnitude of current is different with the current being about 70 nA at a bias voltage of 100 mV. In the case of $Ti_{1-x}Nb_xN$ film with x=0.77, the grain interior and grain boundary contributions can be easily separated since the size is 90 nm. It is seen that the I-V characteristics of all points selected on the grain and grain boundary shows Ohmic behavior. However, the resistance is higher for the point (+2) selected on the grain boundary compared to that of the points (+1 and +3) selected on the grain interior. The magnitude of current is of the order (100 nA) of on the grain interior and is about 70 nA on grain boundary at a bias voltage of 100 mV.

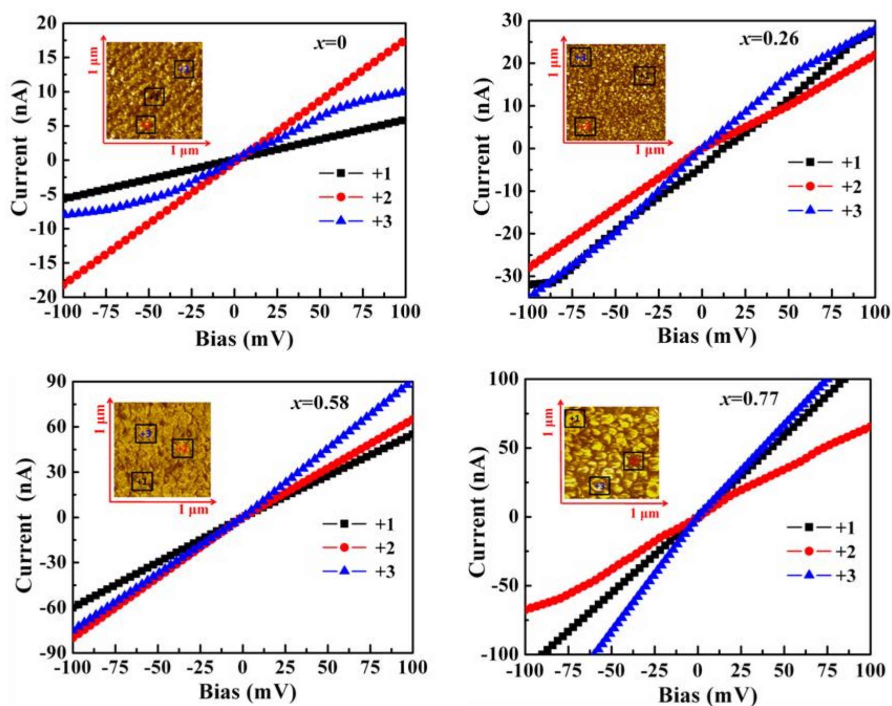

Figure 6.7 Local I-V characteristics of $Ti_{1-x}Nb_xN$ films for a sweeping voltage of ± 100 mV. The 2-D current images with locations at which the I-V characteristics were measured are given in the insets.

6.5.2 Microstructure dependent local resistance

The local resistance of TiN_x and $Ti_{1-x}Nb_xN$ films was calculated from I-V characteristics measured at different locations in each film. The measured local resistance of all films is in the range of MΩ. For $Ti_{1-x}Nb_xN$ films, the local resistance was plotted as a function of mean grains size. Figure 6.8 shows variation of local resistance of $Ti_{1-x}Nb_xN$ film with grain size. It is observed that the local resistance is decreased with an increase in grains size. The local resistance of TiN film for x=0 is 20 MΩ and the value is decrease to 0.05 MΩ for x=077 of $Ti_{1-x}Nb_xN$

film. As compared to the figure 6.1, the variation in local resistance is follow the same trend as composition dependent sheet resistance, but strongly dependent on the microstructure.

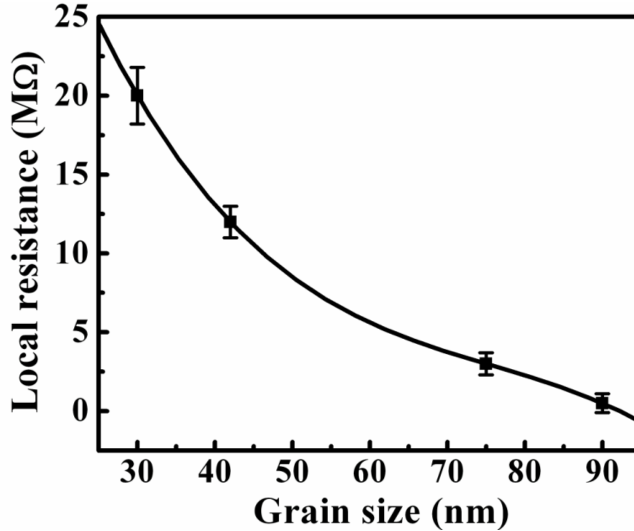

Figure 6.8 Variation in the local resistance of $Ti_{1-x}Nb_xN$ film with grain size.

It is clear from the results presented above that the conductivity in nanostructured TiN_x and $Ti_{1-x}Nb_xN$ films has two major contributors: (1) electronic structure, and (2) microstructure.

6.5.3 Electronic structure

When two materials are electrically connected, electrons flow from the material with the smaller work function to that with the higher work-function. The diffusion current builds a double layer at the interface. This results in a contact potential difference (CPD), $\Delta\Phi$,

between the two materials until the Fermi levels (E_F) for each one are equal. Schematic diagram of variation in Fermi level before and after contact between tip and film is shown in figure 6.9.

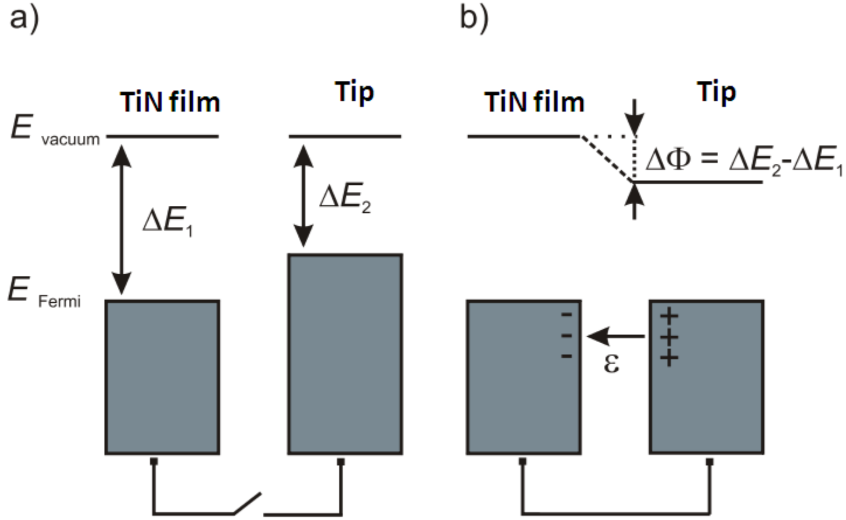

6.9 (a) difference in Fermi level between film and tip before contact (b) equalized Fermi level after contact

Conducting AFM tip and film (TiN_x and $Ti_{1-x}Nb_xN$) with different work-functions are connected, then the CPD is given by [200].

$$\Delta\Phi = \frac{\Phi_{E_2} - \Phi_{E_1}}{e} = \frac{\Phi_{tip} - \Phi_{film}}{e} \qquad (1)$$

The work function of the gold coated tip is ~5.1 eV [201] whereas that for the TiN_x film is ~4.0eV [202]. The CPD is approximately 1 eV and this value is significantly varies for tip and $Ti_{1-x}Nb_xN$ film contact.

The attractive force, F, between the tip and the sample takes the form

$$F = \frac{1}{2}(\Delta\Phi)^2 \frac{\partial C}{\partial z} \quad (2)$$

Where C is the separation-dependent capacitance between the tip and sample and z is the tip-sample distance. The variations in conductivity due to the differences in electronic structure are manifested as changes in the total resistivity as a function of the chemical composition. From eqns (1) and (2) it can be inferred that the local work function can also vary due to local variations in stoichiometry [203-206].

6.5.4 Microstructure

Microstructure dependent variation in electrical resistance can be explained by considering the electron-grain boundary scattering in polycrystalline metallic films based on Mayadas and Shatzkes model. Microscopically there are two main scattering mechanisms that can lead to increase the resistivity of polycrystalline metallic films. The first one is electron-surface scattering described by Fuchs and Sondheimer (F-S) [207, 208]. The second one is electron-grain boundary scattering described by Mayadas and Shatzkes (M-S) [209]. In general, this two scattering mechanisms contributes the resistivity increase, if the films with varying thickness and mean grain size. Both theories are associated with phenomenological parameters with which the resistivity increase can be quantified. The specularity parameter (p) in the first case denotes the degree of elastic scattering at the surface and the grain boundary

reflection coefficient (*R*) in the second case describes the physical nature of scattering at the grain boundary. It is inferred that the grain boundary scattering is the strongest contribution to the resistance increase. In the M-S model, it is assumed that the every grain boundary as an internal surface. When an electron collides with a grain boundary, it has a probability of transmission or reflection that is quantified by a reflection coefficient, *R* ($0<R<1$). The resistivity is dependent on the reflection coefficient for electron transport at the grain boundaries and will therefore increase with an increase in the grain boundary contribution. Figure 6.10 shows the visualization picture of the grains boundary scattering in a polycrystalline thin films.

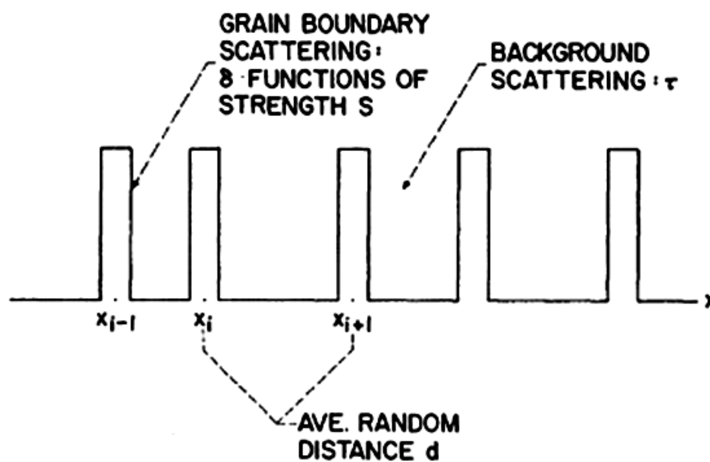

Figure 6.10 Grain boundary scattering representation in Mayadas-Shatzkes model

Clearly, in the TiN as well as the $TiN_{0.76}$ films the filamentary nature of current flow is due to the large reflection coefficients at the grain boundaries, leading to increased grain boundary scattering. Due to

this, electron transport across a grain boundary in the case of $TiN_{0.76}$ film is mainly due to tunneling. As a consequence, the number of percolation paths is low, the barrier for electron transport is high and therefore the total resistivity is high. For $Ti_{1-x}Nb_xN$ thin films, from figure 6.5, it is observed that the grain number density is high for TiN (x=0) film. As a consequence, it has more grain boundaries that contribute to electron scattering as compared to that for $Ti_{1-x}Nb_xN$ films. The probability of electron scattering from grain boundary is higher on TiN (x=0) film and is lower on $Ti_{1-x}Nb_xN$(x=0.77) films. This argument is supported by figure 6.8 where it is seen that the local resistance of TiN (x=0) film having grain size 30 nm is higher than that the $Ti_{1-x}Nb_xN$ (x=0.77) film having grain size 90 nm. It is evident that a change in Nb concentration from 0.28 to 0.77 (roughly 2.75 times) causes less than one order of magnitude change in the resistance (figure 6.1). In contrast increase in grain size from 30 to 90 nm leads to more than two orders of magnitude decrease in the local resistance (figure 6.8). The local variations in resistance can thus be correlated with microstructural variations in the Nb substituted films rather than the variation in Nb concentration. From the figure 6.7, it is evident that the I-V characteristics of the film are not similar, even the point taken on the grain interior of respective film. Adjacent grains with equal size and height have different electrical interaction (strong or weak) depends on the grain boundary width and oxidation states present. These variations could lead to vary the local electrical characteristic of the films. Since the C-AFM measurements were performed at ambient atmosphere, it is possible to present a few nanometers native oxide states on the surface of the films. The variations in the oxidation states play a crucial role on the local electrical and

electron transport properties of the films [196]. The native oxide layer is act as a potential barrier for electron transport. In addition to the grain boundary scattering, local oxidation is also responsible for increase the local resistance.

6.6 Summary

Microstructure dependent local electrical and electron transport properties in TiN_x and $Ti_{1-x}Nb_xN$ thin films studied by conductive atomic force microscopy. In both TiN_x and $Ti_{1-x}Nb_xN$ films the current flow on the surface is filamentary nature. Comparison between the topography and the current maps of TiN_x films of two compositions show that grains in stoichiometric TiN are electrically conductive but those of sub-stoichiometric $TiN_{0.76}$ film are electrically resistive. While in $Ti_{1-x}Nb_xN$ films current map on the surface of the films is varying according to the microstructure. Current on the grain interior is higher than the grain boundary and grain boundaries are act as potential barrier for electron transport. An examination of the I-V characteristics demonstrated that for TiN the I-V curve is almost linear (as for a metal), but for the sub-stoichiometric $TiN_{0.76}$ film, the I-V curve is non linear, which indicates the presence of a high barrier for electron transport across grain boundaries. I-V characteristic of $Ti_{1-x}Nb_xN$ thin films exhibits linear variation indicate that the Ohmic contact between tip and films. Local resistance of TiN_x and $Ti_{1-x}Nb_xN$ films is increased several orders of magnitude as compare to the total resistance. Microscopic electron scattering from the grain boundary and the presence of native oxide layer on the surface is giving rise to the macroscopic resistance.